

Hysteretic elasticity in damaged concrete: Quantitative analysis of slow and fast dynamics

M. Bentahar,¹ H. El Agra,¹ R. El Guerjouma,^{1,2} M. Griffa,^{3,4} and M. Scalerandi^{3,*}

¹GEMPPM UMR CNRS 5510 and INSA de Lyon, 20 Av.A.Einstein-Bât.Blaise Pascal, Villeurbanne, France

²LAUM UMR CNRS 6613 and Université du Maine at le Mans, Av.Olivier Messiaen, Le Mans Cedex 9, France

³CNISM-Dip. Fisica, Politecnico di Torino, C.so Duca degli Abruzzi 24, Torino, Italy

⁴Bioinformatics and HPC Labs, Bioindustry Park of Canavese, V.Ribes 5, Colletterto Giacosa, Italy

(Received 12 April 2005; revised manuscript received 17 November 2005; published 27 January 2006)

Fast and slow dynamics in the elastic response of damaged materials to external excitations show evidence of an anomalous (hysteretic) elastic behavior. Experimental observations may be used to detect and eventually characterize the damaged state of structural components. At the same time, reliable theoretical models might support data interpretation and development of new experiments. Here, we analyze the resonance frequency shift in undamaged and damaged concrete bars, comparing experimental results and theoretical predictions obtained from a Preisach-Mayergoyz based elastic model.

DOI: [10.1103/PhysRevB.73.014116](https://doi.org/10.1103/PhysRevB.73.014116)

PACS number(s): 62.20.-x, 62.40.+i, 83.60.Uv, 81.70.Bt

I. INTRODUCTION

Fast dynamics,¹ conditioning, and slow dynamics² have been shown in the last years to be features shared by the elastic response of several materials, such as rocks,³ damaged materials,⁴ composites,⁵ concrete,⁶ etc. Recently, it has been shown that the anomalous resonance frequency shift with increasing driving amplitude (fast dynamics) disappears at low strains.⁷ The authors have shown that any anomalous frequency shift at a given amplitude is associated with variations of the elastic properties of the specimen (conditioning) which do not disappear immediately when the perturbing amplitude is removed. It is then suggested that perturbations caused by an external wave (or even a temperature change)^{1,8} may shift the material to a nonequilibrium state, hence slow dynamics (i.e., the log time recovery of the resonance frequency after conditioning) may be seen as a relaxation of the specimen to its configuration before the perturbing excitation.⁹

An understanding of the mechanisms responsible for the mentioned anomalous elastic behavior might shed light on the comprehension of the link between hysteresis and damage state,¹⁰ with a consequent wealth of applications in the field of materials characterization. Indeed, nonlinear signatures are the first manifestations of the presence of damage in materials.¹¹

Nevertheless, some drawbacks for application of techniques based on fast dynamics are immediately evident. In fact, a large elastic energy must usually be injected in the specimen (which is not always easy) to obtain small effects, hardly measurable *in situ*, e.g., a resonance frequency of a few percentage points.^{1,10,12} Furthermore, the nonlinear properties of hysteretic media are very sensitive to environmental conditions, such as temperature,⁸ humidity, confining pressure,¹³ etc. On the other hand, it is much easier to perform measurements based on the detection of slow dynamic effects, which seem to be equally (or even more) sensitive to damage.^{4,5} Here parameters as the typical time scale of the recovery process are expected to be optimal indicators for damage detection.

However, a further step is in any case necessary, i.e., the linking of the nonlinear parameters (either in the fast or slow

dynamics) to the damage properties and to the life expectancy of the component under examination. Attempts have recently been made in this direction,¹⁴⁻¹⁷ but, to our knowledge no definitive and reasonable conclusion has been reached so far. Hence mathematical models to describe hysteresis should be derived mostly from phenomenological observations.

Nevertheless, even phenomenological descriptions can support data interpretation and experiments optimization. With this purpose, several models have been proposed in the last decade^{9,14,18-24} to capture the phenomenology of wave propagation in hysteretic elastic media. Most of them are based on a Preisach-Mayergoyz (PM) approach,^{25,26} in which the material properties at a mesoscopic level are obtained from the collective behavior of simple units (hysteretic elements, HE), with a two-state behavior. We have introduced a description based on some hysteretic elastic elements (HEE), with different elastic constants in the two states.^{9,22} This feature makes our approach different from others, that are based on units with both states rigid and differing only in their length (hysteretic mesoscopic units, HMU).^{18,21}

While all the proposed approaches capture the phenomenology relative to fast dynamics well (and to quasistatic experiments also), more complex is describing slow dynamics and conditioning. So far, only models based on HEE's have been proven capable of linking conditioning and fast dynamics^{9,22,27} and to easily introduce relaxation phenomena.^{9,28} To our knowledge, only a model recently proposed by Vakhnenko *et al.*,¹⁴ but not based on a PM approach, have obtained a similar agreement with the phenomenology.

In this paper, we will focus on considering resonance frequency experiments in concrete, which is known to be slightly nonlinear and hysteretic even when not damaged.²⁹ In our work, we wish to compare the sensitivity and accuracy of fast and slow dynamic measurements to the presence of damage. To support the analysis, considerations arising from a proposed model will be used, after validation of the reliability of the approach through a quantitative comparison of theoretical and experimental data.

In the next section the performed experiments will be discussed and the experimental setup described. The model, already partly presented elsewhere, will be briefly discussed in Sec. III and numerical and experimental results will be presented and compared in Sec. IV. Finally, some model-based interpretation of the data will be suggested and the emerging lines of investigation outlined.

II. EXPERIMENTAL SET UP

A. Specimen

We consider here small concrete bars of cross section $\Sigma = 10 \text{ mm}^2$ and length $L=61 \text{ mm}$. Several specimens have been produced with an identical treatment. One of them (intact specimen) has been used for reference, while other sets have been damaged through compression tests, up to the yield rupture, determined to be about 65 MPa. Longitudinal and transverse velocities in the intact sample have been measured to be $v_L=3389.6 \text{ m/s}$ and $v_T=2217.3 \text{ m/s}$, corresponding to a Young's modulus of 24 GPa and Poisson ratio of 0.126. Density is $\rho=2167.6 \text{ Kg/m}^3$.

A porosity meter is used to determine the density of pores with a volume fraction corresponding to 14%. Pores sizes change from 0.5 to 315 μm . Concrete samples have no preferential grain orientation. Cracks, which are present even in the intact state, could have lengths up to 2 mm with an opening corresponding to few microns. It follows that interstices can be assumed to be much smaller than grains (of the order of one with respect to tens of μm).

Nonlinear properties of concrete samples have been previously investigated by several authors.^{3,6,29-31} Nevertheless, most of the experiments performed so far were aimed to analyze the elastic properties of the sample in propagation condition, e.g., through a spectral (nonlinear) analysis^{6,30} or using actively modulated acoustic signals.³¹ Only few experiments have been performed in resonance conditions.³ Here, however, a rigorous analysis of damage effects have not been addressed. Furthermore, experiments of both fast and slow dynamics in correlation with damage on the same material are not reported elsewhere, to our knowledge.

B. Experimental setup

The experimental set-up is presented in Fig. 1. It is based on the following principle: the gain-phase analyzer generates a continuous sinusoidal wave, while performing frequency sweeps to excite the material around its natural vibrating modes. The signal amplitude is controlled by the analyzer and amplified with a constant gain. At one extremity of the sample (suspended to have free boundary conditions at both ends) we attached one piezoelectric transducer to produce in the sample ultrasonic vibrations, which are revealed at the other tip through a laser vibrometer. The analyzer displays the received signals and transmits them to the computer for data processing. The method could be readily adapted to samples having particular geometries.

As the aim of this work is to detect material nonlinearities for weak strains (vibrations), we have taken great care to minimize nonlinearities due to electronics, in particular, by

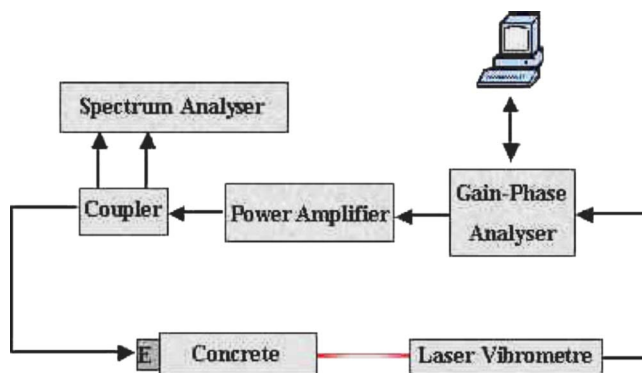


FIG. 1. (Color online) Experimental setup used for the nonlinear characterization.

using a high power ultrabroadband coupler connected to a spectrum analyzer. Indeed, the latter displays the spectrum of reflected and transmitted signals through the coupler, allowing us to control possible distortions due to electronics, which leads to a better adjustment of the experimental device.

The linearity of the experimental device was also tested on an intact aluminium sample whose nonlinearity is of the “atomic order.” For an accuracy corresponding to 0.1 Hz, the reference material has proved to be linear until an excitation corresponding to a longitudinal strain $|\epsilon|=10^{-5}$, beyond which the resonance frequency shifts for electronics reasons (i.e., influence of the electronics chain on the measurements). This nonlinearity threshold is sufficient to study the nonlinear behavior of concrete, since heterogeneous materials behave nonlinearly for lower strains. Indeed, measurements on the concrete samples have always been performed well below such threshold, with an additional check provided by the coupler (not used in previously reported experiments²), which warrants a careful test of the linearity of the electronic chain.

C. Experiments

In the performed experiments, the resonance frequency of the specimen (damaged and undamaged) has been measured under different conditions, as will be discussed below. Resonance curves have been obtained by sweeping the frequency around the sample first compressional vibrating mode (located at about 26 KHz) and recording the vibration velocity of the tip of the bar opposite to the one on which the transducer is attached. Data processing then allowed to extract the averaged vibration velocity at the sample tip.

Two sets of experiments have been performed:

(i) Fast dynamics experiments: successive resonance curves have been measured for different excitation amplitudes, without letting the system relax during the experiment. Here, voltages from 10 to 100 mV have been amplified before exciting the material. To obtain enough energy in the sample, we have used a constant gain corresponding to 52 dB. As the input channel of the gain phase analyzer is conceived for small voltages, the output signals were divided by a factor of 10, which corresponds to an attenuation of 20 dB.

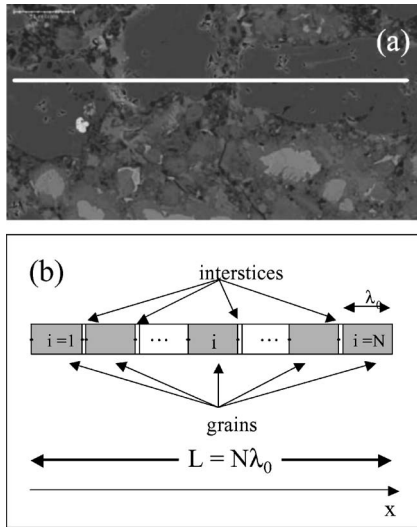


FIG. 2. (a) Microphotograph of a $110 \times 40\text{-}\mu\text{m}$ section of the intact concrete bar; (b) its schematic representation.

(ii) Slow dynamics experiments: the gain phase analyzer is set at a fixed tension of 10 mV. For a short time duration, the amplifier is switched on (52-dB amplification) to obtain a large amplitude signal in the sample, which induces conditioning. Afterwards, the amplifier is switched off and the resonance frequency is tracked in time every 50 (10–100) secs in the case of intact (damaged) samples.

In the chosen conditions the experimental device is linear. Thus the stress σ_{ext} applied by the piezoelectric transducer on the specimen surface is linearly dependent on the tension V generated by the gain phase analyzer. In this case it would be possible to define an efficiency coefficient g and link the stress to the tension as

$$\sigma_{ext} = gV. \quad (1)$$

It should be noted that the coefficient g depends on the considered setup. Indeed, the acoustic impedance of the system may change either by switching on the amplifier or by changing sample (damaged and undamaged in our study). As such, it does depend on the acoustic properties of the specimen (density and Young modulus), on the properties of the full electronic chain and on the quality of the specimen surface. It follows that the transduction efficiency is altered and should not be taken as unchanged for the different experiments or dependent only on the acoustic impedance of the specimen.

III. THEORETICAL MODEL

As discussed in the previous section, experiments have been performed on small concrete bars with negligible cross section Σ to length L ratio. Since compressional waves are used with rather large piezoelectric transducers, a one-dimensional (1D) description is sufficient to model wave propagation.

Furthermore, concrete is known to have a complex microstructure, in which grains alternate with interstitial regions [see Fig. 2(a)]. It is then reasonable to schematize the mate-

rial as a sequence of alternating hard (grains) and soft (interstices) portions, with different equations of state [see Fig. 2(b)]. The porosity of the specimens considered is about 14%. It follows that interstices can be assumed to be much smaller than grains (of the order of one with respect to tens of μm).

A. Equations of state

Experimental findings have clearly shown the source of nonlinearity to be localized in the soft portions, either directly as nonlinear properties of the interstitial materials¹ or as a consequence of rough contacts between grain asperities.^{16,32} It follows that the stress σ acting on the grains is described by the usual viscoelastic equation

$$\sigma = E\varepsilon + \eta\dot{\varepsilon}, \quad (2)$$

where E is the Young modulus, η the viscoelastic coefficient and the strain is $\varepsilon = \partial u / \partial x$ (u is the displacement). A dot denotes as usual a time derivative.

All the nonlinearity is then confined to the interstices, from now on identified as hysteretic elastic elements (HEEs). We adopt here a phenomenological equation of state in which the stress τ supported by the interstice is linked to the pressure P confining the interstice (applied by the surrounding grains) and to the interstice strain δ . The equation of state, similar to that for poroelastic media,³³ is

$$\tau = -\frac{a_1}{2}P + a_2\delta + a_3\dot{\delta}, \quad (3)$$

where the values of the three parameters a_i ($i=1, 2, 3$) determine the HEE state. Further details can be found in Refs. 9 and 28.

B. Bi-state description of the interstices

Following a Preisach-Mayergoyz (PM) space approach, we assume the interstice to occupy one of two allowed states: a “closed” ($a_1=1.0$, $a_2=0$, $a_3=a_{3r}$) and an “open” ($a_1=a_{1e} < 1.0$, $a_2=a_{2e} \neq 0$, $a_3=a_{3e}$) state. The closed state is rigid, i.e., the strain does not change with time, since at any time the stress supported by the HEE is equal to the applied pressure [see Eq. (3)]. On the contrary in the open state the interstice length varies with time according to the applied pressure.

Rules for the transition between the two states are driven by the pressure applied to the interstice. It is sufficient in this context to follow the usual deterministic description,^{9,26} rather than more complex protocols.³⁴ We introduce, for each interstice, a different pressure pairs (P_c, P_o) , with $P_c > P_o$. The set of pairs gives a distribution in a 2D state space called PM space, which characterizes the system. Starting at a pressure $P < P_o$, the interstice is in the open state, up to the pressure P_c where it switches to rigid. When P decreases, transition to the elastic state occurs at $P = P_o$: see Fig. 3(a).

Nonlinearity of the system is then generated by transitions between the two states. It follows that the three parameters $\{a_{ie}\}$ are indicators of the intrinsic nonlinearity of the specimen. In particular, the further they are from the rigid state

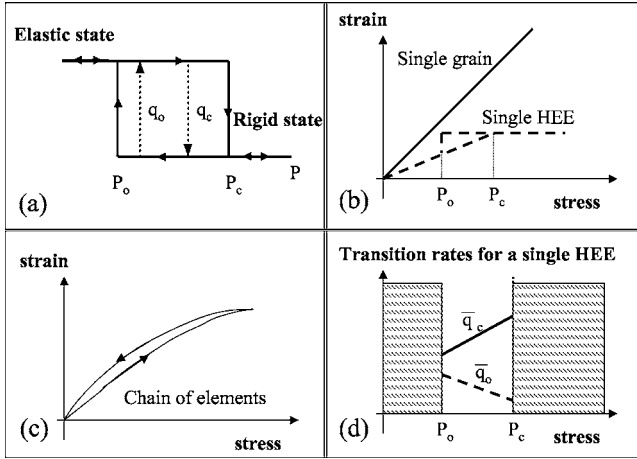


FIG. 3. (a) Representation of the bi-state protocol adopted for the hysteretic elements; (b) stress-strain relation for a single grain (linear) and a single HEE (bi-state function); (c) stress-strain relation for a chain of alternating grains and HEEs; (d) representation of the transition rates as a function of the pressure applied to the HEE. Transition rates cannot be defined in the dashed regions, where only one state is allowed [see also Fig. 3(a)].

values, the more the system is nonlinear (or damaged). Note that cross correlations in the role of the parameters are present, making the classification of the system properties complex, as it will be discussed in the next section.

Also the distribution of the pairs (P_c, P_o) in the PM space affects the hysteretic properties of the system. Here, we limit ourselves to considering a uniform distribution in the range $-P_{max} < P_{c,o} < P_{max}$.

The schematic stress-strain behavior of grains and HEEs is reported in Fig. 3(b) (for a single grain/HEE) and in Fig. 3(c) for a chain of alternating grains and HEEs. The single HEE is described by an *ad hoc* mathematical equation of state, while the chain provides a meaningful physical stress-strain relation. More details can be found in Ref. 22.

C. Relaxation processes in the bi-state formalism

From the description introduced above, it is evident that the HEE is in a well defined equilibrium state (rigid or poroelastic, respectively) only when the applied pressure is larger than P_c or smaller than P_o . In the intermediate pressure range, two states are possible and the actual state of the system is determined by the previous stress history [see Fig. 3(a)]. It is then reasonable to introduce random transitions between the two “coexisting” states, with probabilities (per unit time) q_c and q_o for the transitions to the rigid or to the elastic state, as introduced in Ref. 9. The fact that relaxation always corresponds to hardening, as we will discuss later, suggests the assumption $q_c > q_o$, in agreement with the observation that more energy is needed to break a rigid (closed) bond, in which static features may be at play.

With respect to previous approaches,^{9,28} we consider here a dependence of the probabilities on the shape of the bi-state loop. Indeed, if the HEE is kept at a pressure P , jump probabilities should depend on the differences $|P - P_{c,o}|$. In fact, relaxation probabilities depend on the difference between the

energy levels of the two states and, in a first approximation, we assume them to vary linearly with the external loading (P in our case). Therefore since transitions from one state to the other are expected to be easier when the pressure is close to the corresponding deterministic transition, we adopt the following definition for the effective transition rates:

$$\bar{q}_{c,o} = q_{c,o} \left(1 - \frac{|P - P_{c,o}|}{2P_{max}} \right) \quad \text{when } P_o < P < P_c. \quad (4)$$

The transition rates are schematically reported in Fig. 3(d) for one HEE as a function of P . $\bar{q}_{c,o}$ are not defined in the region outside $P_o < P < P_c$, where only one state is allowed [see Fig. 3(a)]. Here, e.g., for $P > P_c$, the HEE is always in the rigid state and transitions are no longer allowed (equivalent to $\bar{q}_c = 1$ and $\bar{q}_o = 0$).

It is also to be noted that, as in previous papers, we consider here isothermal processes, hence dependencies on temperature are neglected.

The relaxation process defined allows the introduction of the initial configuration of the system in a nonarbitrary way. Considering that numerical experiments are assumed to be performed, as in experiments, on a completely relaxed specimen (i.e., kept at $P=0$, constant temperature and humidity for a very long time), all the HEEs are initially at their rest-length state. Units with $P_o < P_c < 0$ are in the closed state, while units with $P_c > P_o > 0$ are open. The remaining elements are in the closed/rigid state with probabilities $\bar{q}_{clo}/(\bar{q}_c + \bar{q}_o)$, respectively.

IV. RESULTS

In this contribution, we will present results concerning both fast and slow dynamics experiments, as presented in Sec. II. Both theoretical (details about the numerical implementation are reported in the Appendix) and experimental data will be shown, in the case of an intact and a damaged concrete sample. The linear parameters of the specimen have been measured: bar section $\Sigma = 10 \text{ mm}^2$; sample length $L = 61 \text{ mm}$; Young’s modulus $E = 24 \text{ GPa}$, density $\rho = 2167.6 \text{ Kg/m}^3$. Furthermore, we have considered $\eta = 250 \text{ Pa sec}$, corresponding for these parameters to a linear Q factor of about 570, reasonable for concrete. Note that attenuation will be influenced also by nonlinear contributions already at low excitation amplitudes. We consider grains and interstices with typical dimensions $\varepsilon_0 = 75 \mu\text{m}$ and $\delta_0 = 1.5 \mu\text{m}$, respectively, for a total of $N = 810$ discretization nodes in our numerical approach.

The set of parameters to describe the nonlinearity have been chosen to obtain a best fitting of the experimental data. As a result of an extensive analysis, the coefficients in the poroelastic state have been chosen as $a_{1e} = 0.9995$, $a_{2e} = 48 \times 10^{-5} \text{ GPa}$; $a_{3e} = 14 \text{ Pa sec}$ for the intact state (i.e., a small nonlinearity). For the damaged state, to simulate more nonlinearity, $a_{1e} = 0.98725$, $a_{2e} = 156 \times 10^{-5} \text{ GPa}$; $a_{3e} = 7 \text{ Pa sec}$ have been chosen. Furthermore, the relaxation parameters used in the simulations are $q_o = 5.4 \times 10^{-6}$, $q_c = 8 \times 10^{-4} \text{ events/sec}$.

The choice of the “best fitting” set of parameters has been performed by first adjusting them in order to fit the reso-

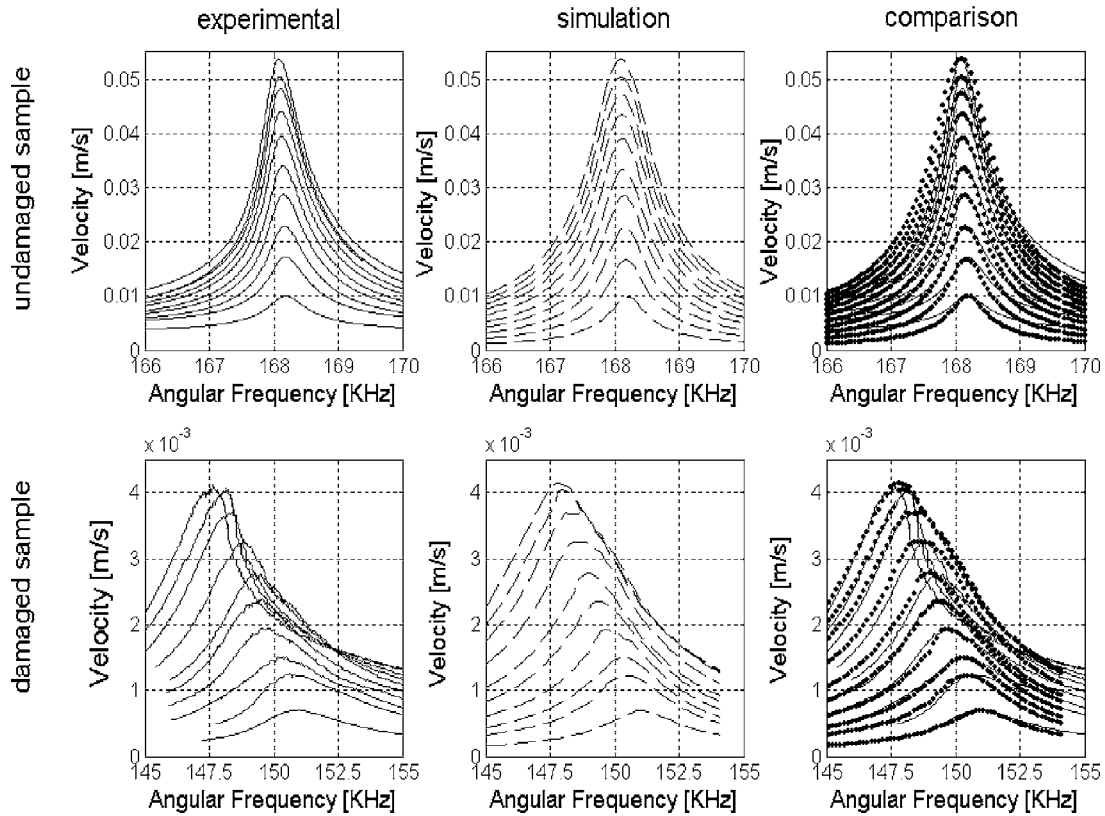


FIG. 4. Experimental and theoretical resonance curves for undamaged (first row) and damaged (second row) samples at ten different excitation amplitudes (from 10 to 100 mV). For better visualization a comparison is presented superimposing, in the last column, experiments and simulation data.

nance curve at the lower excitation amplitude. The resonance frequency is sensitive only to a_{1e} and a_{2e} (ω_r decreases with decreasing a_{1e} or a_{2e}), while a_{3e} plays only to define the amplitude at resonance. Fitting of the curves at larger amplitude gives then only a slight adjustment of the parameters a_{1e} and a_{2e} . It is important to observe also that numerical results are very sensitive to the choices of the parameters. For instance, a 1% change in a_{1e} gives a change in the resonance frequency ω_r of about 10%.³⁵

In experiments the various curves correspond to different voltages applied to the generator (varying from 10 mV to 100 mV). We have assumed, for the intact case, an efficiency conversion factor $g=54 \times 10^3 \text{ Pa V}^{-1}$ [see Eq. (1)]. It follows that the driving amplitude σ_{ext} used in the simulations varies from 540 to 5400 Pa.

During the damage process, i.e., when the sample is under stress, some areas behave as stress concentration zones characterized by a high strain level comparing with the rest of the other regions. This allows creation and nucleation of microcracks in the bulk and near the surface even for moderate stress values, which causes a change in the material's impedance and decreases the efficiency of the coupling effect. As a consequence, in the simulation for the damaged case we have used a smaller efficiency $g=27 \times 10^3 \text{ Pa V}^{-1}$.

A. Fast dynamic experiments

In Fig. 4, results from a fast dynamic experiment, i.e., the

determination of the resonance frequency for different values of the driving amplitude σ_{ext} , are reported. The experimental data and simulation results (first two columns) show a good quantitative agreement, for both the undamaged and damaged samples, as highlighted in the third column where the experimental (solid lines) and theoretical (dots) curves have been superimposed.

Data show that already in the intact case (first row), the sample is slightly nonlinear. Both experiments and simulations show in fact a small shift of the resonance frequency to the left (here it is hardly visible, but see also Fig. 5) when increasing the forcing (larger σ_{ext}). More evident is the contribution of nonlinearity to attenuation: the ratio of the peak amplitudes at resonance for the lower and higher injection amplitudes is about 9 (considering offsets), i.e., well different than the ratio of 10 of the corresponding injected amplitudes. Further evidence of nonlinear attenuation is given by the increase of the curve width with increasing the excitation amplitude. The simulation results agree well with experimental data. In particular, the resonance frequencies and the peak velocity values are very well estimated, even from a quantitative point of view. Slightly more approximate is the prediction of the curve width, which, in the simulations, is slightly smaller at low amplitude and larger at high amplitude. Nevertheless, as will be discussed in Fig. 6, the agreement is satisfactory.

Similar considerations are valid for the damaged specimen (second row of Fig. 4). In this case, however, the effect

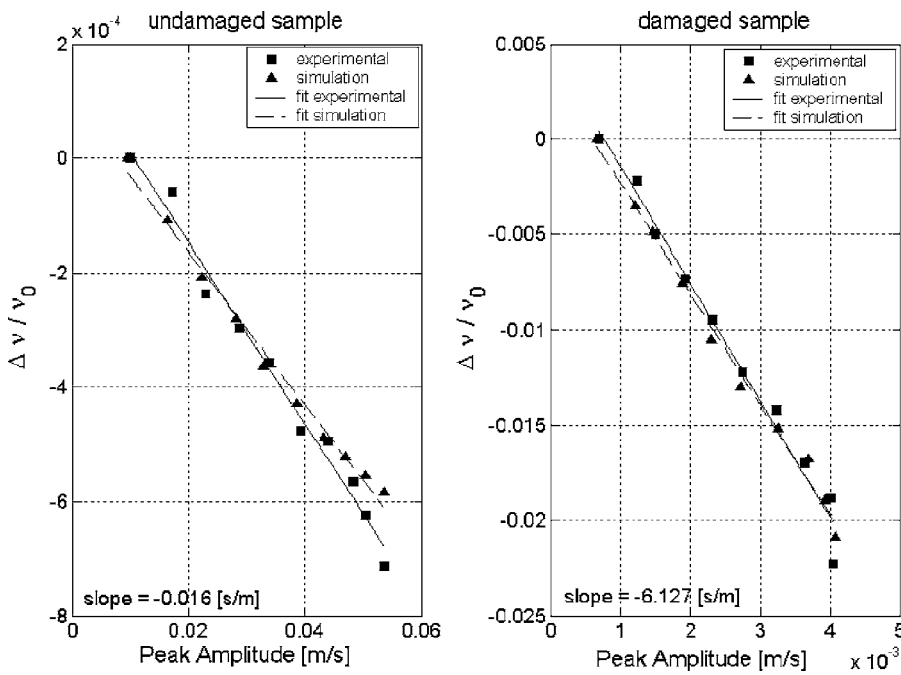


FIG. 5. Resonance frequency shift as a function of the peak amplitude. Experimental (squares) and model (triangles) data are fitted by a straight line (with slope reported in the plot) for both the undamaged and damaged samples.

is much larger and more easily distinguishable (note the different scale in the angular frequency scale). Also, besides the shift and increase in attenuation, resonance curves are considerably distorted from the classical Lorentzian shape, as qualitatively captured from the simulations. Again, optimal quantitative agreement is found for the peak values and resonance frequencies at the different values of σ_{ext} , while satisfactory agreement is found for the width of the curves.

The same observations are reported in Figs. 5 and 6 in a more quantitative way. Here we plot, as a function of the peak amplitude (averaged velocity at resonance), the relative resonance frequency shift (Fig. 5) and relative Q -factor change (Fig. 6), defined as

$$\frac{\Delta\omega_r}{\omega_r} = \frac{\omega_r(\sigma_{ext}) - \omega_{r0}}{\omega_{r0}},$$

$$\frac{\Delta Q}{Q} = \frac{Q(\sigma_{ext}) - Q_0}{Q_0},$$

where $\omega_r(\sigma_{ext})$ is the resonance frequency at excitation amplitude σ_{ext} and ω_{r0} is the resonance frequency at the minimum excitation amplitude used ($\sigma_{ext} = g \times 10$ mV). The Q factor has been estimated by the ratio between the resonance frequency and the width of the resonance curve at $\sqrt{2}/2$ peak amplitude. Both quantities behave linearly (note the linear

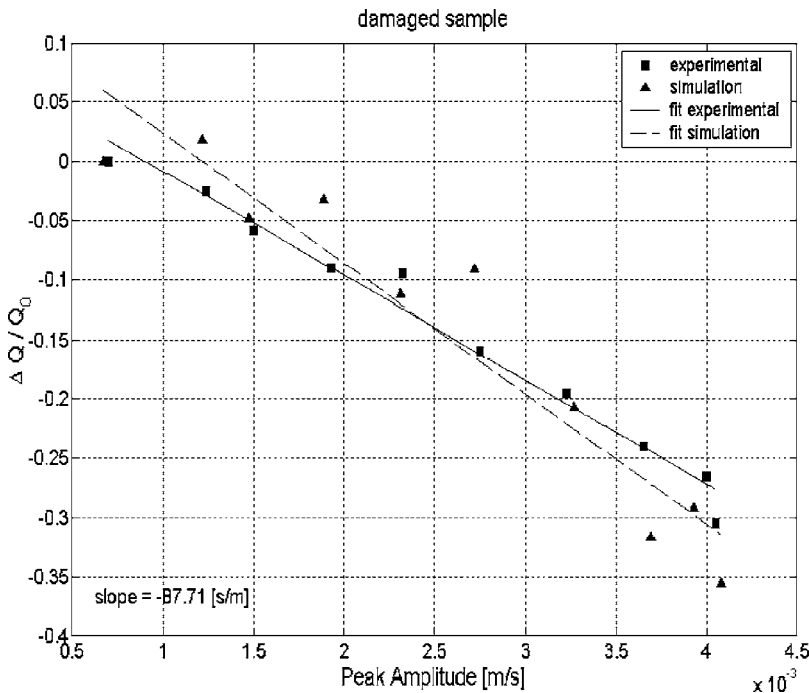


FIG. 6. Q -factor change as a function of the peak amplitude. Experimental (squares) and model (triangles) data are fitted by a straight line (with slope reported in the plot) for the damaged sample.

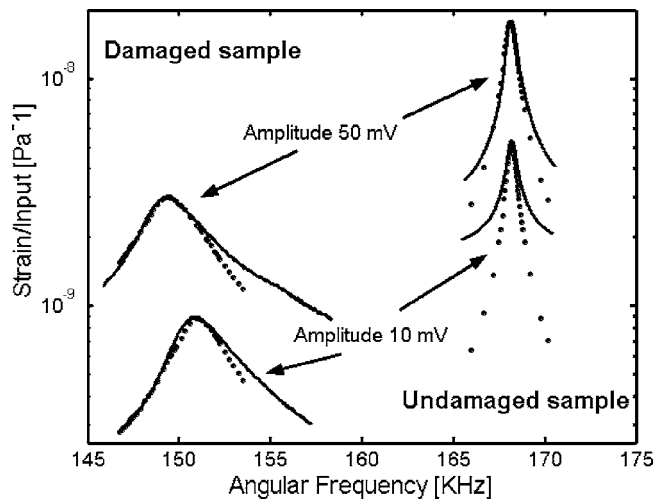


FIG. 7. Strain vs frequency curves for the damaged and undamaged samples at 10 and 50 mV excitation amplitudes. Note the log scale on the y axes.

fitting of the experimental data reported as a solid line) with a good agreement between experimental (squares) and theoretical (triangles) results. Both in the damaged and undamaged cases, the material softens with increasing amplitude and the Q factor decreases (more attenuation). Nonlinear effects are, however, much larger in the damaged case (slopes of the fitting curves are reported in the figures). It is remarkable to note that the change in slope with respect to the intact case is about 400 for the resonance frequency shift and only 3.5 for attenuation.

Finally in Fig. 7 we report the strain (normalized to the input amplitude) vs frequency curves for the damaged and undamaged samples at 10 and 50 mV excitation amplitudes. Results allow us to appreciate the huge effect on attenuation and resonance frequency caused by the damage process. Note that the apparent discrepancy in the tails of the curves for the undamaged case is emphasized by the log scale used.

B. Slow dynamics experiments

As discussed before, in a slow dynamics experiment, the resonance frequency is tracked in time at a fixed amplitude after a larger amplitude wave has been applied to condition the specimen. In Fig. 8, the response of the system during relaxation is reported for a simulation case referring to the damaged concrete specimen excited at 10 mV. In the reported simulation, conditioning is applied at $t=0$ with a 40-mV driving. Resonance curves are reported at successive times after conditioning. As expected, the material is softened by the large amplitude perturbation, but the effect is completely reversible and the resonance frequency slowly recovers its unperturbed value, i.e., the value assumed before conditioning.

The agreement between numerical and experimental data is quite good for both the undamaged and the damaged case. In Fig. 9, the resonance curves at three selected times (for both intact and damaged samples) are reported. Simulations capture well the recovery of the resonance frequency (which

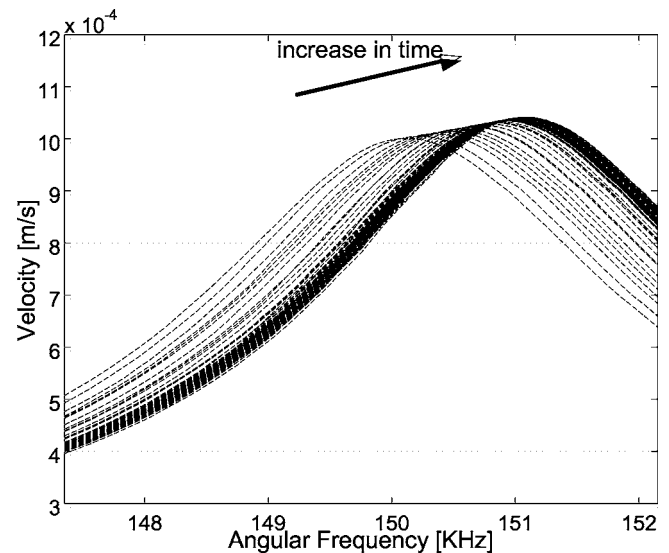


FIG. 8. Resonance frequency curves (simulation) for the damaged sample during recovery after a large amplitude perturbation. The various curves correspond to successive times (the arrow indicates increasing times) during slow dynamics.

is well predicted at all times). Qualitatively the reduction of nonlinear attenuation with increasing time is also well reproduced by the model proposed, even though with some approximation, as already discussed about fast dynamics experiments. Qualitatively the behavior looks very similar for the undamaged and damaged case, due to the slight hysteretic nonlinearity generated by cracks which are already present in the undamaged concrete specimen.

Quantitatively, however, the effect is considerably more evident for the damaged case, as shown in Fig. 10, where the resonance frequency is plotted vs time. The shift after conditioning increases from 0.02% (about 30 Hz) to 0.7% (about 1 KHz) and the recovery time from 5000 to 8000 sec when damage is present. It is to be noted that the recovery, in both experiments and simulations, is logarithmic with time, as found in slow dynamics experiments on several other materials.⁴

V. DISCUSSION

We have presented here some experimental results about resonance frequency measurements in concrete to compare the response of intact and damaged concrete specimens. We have shown that fast and slow dynamics in the elastic response of damaged materials to external excitations show evidence of anomalous (hysteretic) elastic behavior. We have also suggested a model, which captures quantitatively the observed phenomenology, both in fast and slow dynamics experiments. Numerical results have been compared with experimental data, showing a reasonably good agreement. Improvements in the fitting can of course be obtained, in particular for what concerns the prediction relative to attenuation. Nevertheless, in our opinion, a finer search in the parameter space becomes reasonable only once a direct connection of the model parameters with physical properties

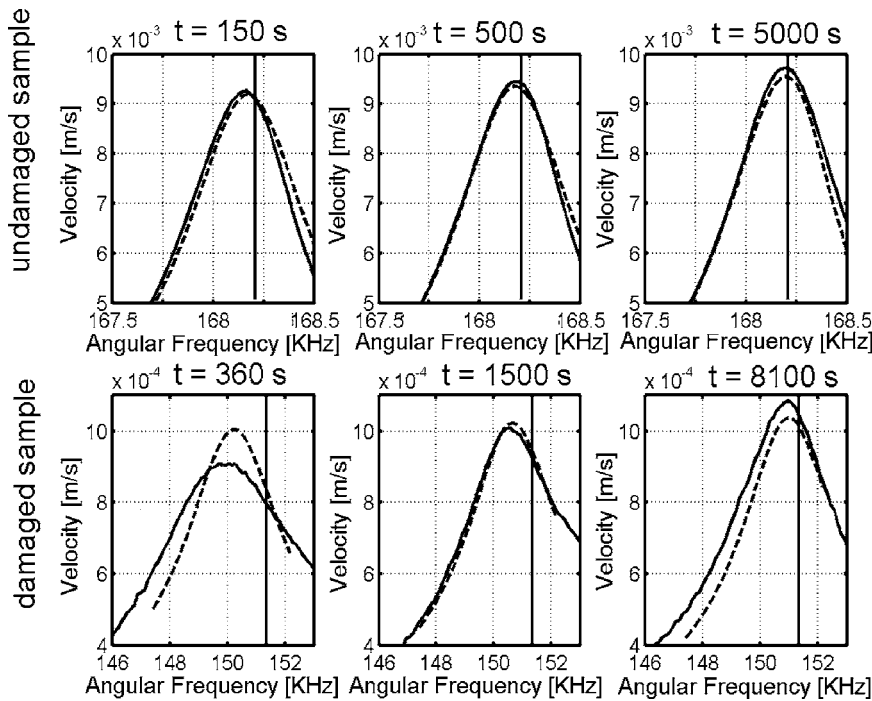


FIG. 9. Experimental (solid line) and theoretical (dash) resonance frequency curves at selected times during recovery for both intact (upper row) and damaged (lower row) samples.

of the damaged zones is proposed and this was not the purpose of the present paper.

Experiments highlight the large sensitivity of the hysteretic nonlinearity to the presence of damage. Indeed, even though concrete presents hysteresis already in its intact state,²⁹ effects are much enhanced for damaged specimens.

In particular, we have found a change of about 400 of the slope of the resonance frequency vs amplitude curve when damage is present. Similar changes, albeit less huge, have also been found for the measured Q factor. Likewise, the parameters characterising conditioning and slow dynamics (frequency drop and recovery time) are also hugely influ-

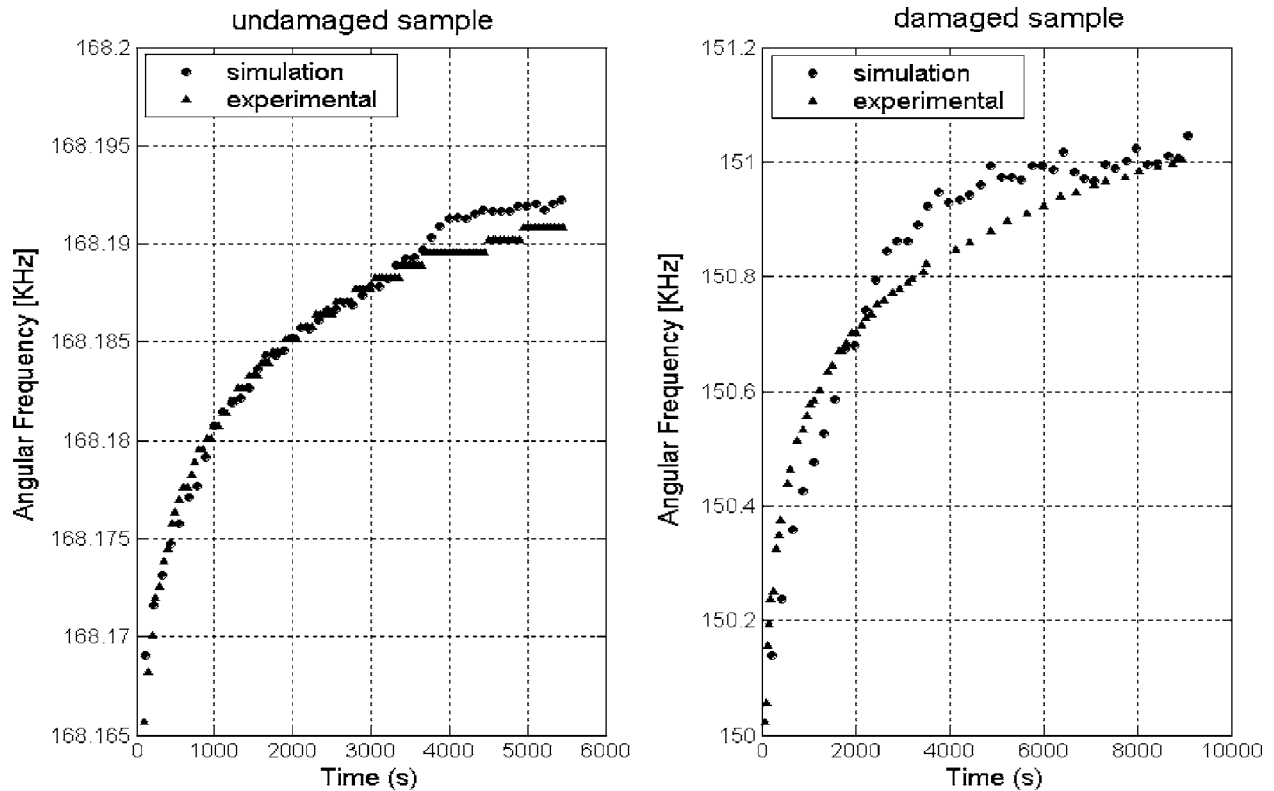


FIG. 10. Resonance frequency vs time during recovery. Theoretical and experimental data are compared for both intact and damaged sample. Note the different scales on both x and y axes.

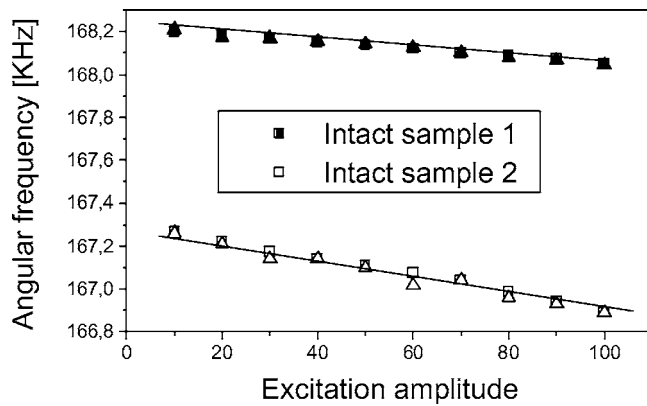


FIG. 11. Resonance frequency vs input amplitude for two intact concrete specimens. Experimental (squares) and model (triangles) data are compared. For both specimen, a linear fitting is also reported.

enced by the presence of damage: about a factor 35 and 2 for the mentioned parameters.

As far as fast dynamics experiments are concerned, it should be noted that, at the lowest amplitude, a considerable change (about 10%) of the resonance frequency may be observed in the damaged specimen (see Fig. 7). This result suggests good sensitivity of a linear measurement to the presence of damage. Nevertheless, a linear measurement of this kind implies a comparison with a “identical” reference specimen, which may not be easy to render available. For instance, small variations during the specimen production may well cause variations of the resonance frequency which might be taken as evidences of small damaging. An example is reported in Fig. 11, where the resonance frequency is plotted vs amplitude for two distinct intact concrete bars, which should indeed be identical. From Fig. 11 it can be easily evinced that the low amplitude resonance frequency drops for the second specimen of about 0.8%, while the slope of the curve vs amplitude is mostly unaffected.

Experiments also show that slow dynamics measurements are easier to perform than fast dynamics ones, but are equally sensitive to the presence of damage. It follows that the drop of the resonance frequency due to conditioning may be a good indicator of damage, together with the recovery time, which, however, is more time consuming to measure.

From a theoretical point of view, the proposed model here is only phenomenological. Nevertheless, if at this stage it does not include any physics, some hypotheses may be formulated from the approach adopted. In particular, about the role of conditioning, i.e., of small (fully reversible) changes of the microstructure when even small amplitude waves are injected in the specimen. Such modifications, corresponding in our model to a modification in the distribution of the initial states of the hysteretic elements composing the specimen, are reflected into a modification of the elastic properties of the material, since the two states of the HE have a different effective elastic constant (for more details, see Refs. 27 and 28).

It follows that, in the model proposed, conditioning effects are also responsible of the anomalous fast dynamic effects, i.e., the resonance frequency at a given amplitude de-

pends on the microstructure as it is “conditioned” at that forcing amplitude. Such a hypothesis about the mechanisms at play seems to be confirmed by recent experimental data,⁷ which point out the impossibility to separate fast dynamics and conditioning in rock samples. Then, slow dynamics follows as a natural relaxation of the system, in which the original microstructure is recovered. Note that here recovering is intended as a recovery to an equivalent, rather than to the very same initial structure.²⁷ At the moment we are aware only of one alternative proposed mechanism,¹⁴ which accounts for slow dynamics.

Finally, we wish to remark here that additional experimental studies have been performed by some of us,⁵ showing very similar effects in composite materials. At the same time, experimental studies are conducted to link slow dynamics with the intensity of acoustic emission events during the processing of damaging of the specimen. Likewise, from a theoretical point of view, several applications of the current model have been proposed elsewhere, e.g., to validate from a qualitative point of view, the validity of the approach to capture other aspects of the observed phenomenology. Nevertheless, far more important from the physical point of view is the progress towards a connection of the proposed approach with physical models.^{16,23}

ACKNOWLEDGMENTS

We wish to thank Professor P. P. Delsanto and Dr. F. Bosia (Politecnico di Torino, Italy) and Dr. V. Tournat (Université du Maine) for useful discussions and Dr. P.A. Johnson (Los Alamos National Laboratory) for his encouragements and suggestions in the experiments setup. This work has been partly supported by EC (AERONEWS Grant No. FP6-502927).

APPENDIX: NUMERICAL IMPLEMENTATION

Equations of motion can be easily derived from the equations of state (2) and (3). Here, we limit ourselves to derive and discuss the equation of motion for the grains. We have

$$\rho \dot{v} = \frac{\partial \sigma}{\partial x} = E \frac{\partial^2 u}{\partial x^2} + \eta \frac{\partial^2 v}{\partial x^2} \quad \text{in grain regions,} \quad (\text{A1})$$

where $v = \dot{u}$ is the vibration velocity and a dot denotes partial time derivative.

The chosen equation of state for the grain regions refers to the Kelvin-Voigt viscoelastic body and is suitable to describe media with quality factor Q inversely proportional to frequency. Concrete samples are known to exhibit a frequency independent Q . As a consequence, it may seem more suitable to use more complex equations of state approaches, which have been developed for modeling frequency-independent attenuation in solid materials. Among them we have analog mechanical models based on the so-called standard linear solid (SLS),^{36–38} or models based on fractional calculus.^{39–41} Nevertheless, in our analysis we are probing the material close to one of its resonance modes, using monochromatic waves in a very narrow frequency band (of width of a few % of the center frequency). It follows that, in such small inter-

val, frequency dependence of attenuation may be considered not influent on the numerical results and a simpler model of the constitutive stress-strain relation, as the Kelvin-Voigt's one, can be considered an acceptable approximation of the mentioned more complex models.⁴²

Once the equation of motions are defined in each element, continuity of both stress and displacements at the boundaries between grains and interstices defines the boundary conditions. Boundary conditions for the left edge of the first grain

(i.e., at $x=0$) include a sinusoidal external forcing $\sigma_{ext} = A_{ext} \cos(\omega_{ext}t)$ while free boundary conditions are chosen for the right tip of the last grain of the sample. The system is then solved numerically, by discretizing space and time. Details may be found elsewhere.^{9,28} Here we limit ourselves to mention that discretization is performed respecting the geometry of the system, i.e., we use two alternating space steps, one corresponding to the grain space scale and the other to the HEE space scale.

*Author to whom correspondence should be addressed. Email address: marco.scalerandi@infm.polito.it

- ¹R. A. Guyer and P. A. Johnson, *Phys. Today* **52**(4), 30 (1999); V. Zaitsev, V. Gusev, and B. Castagnede, *Phys. Rev. Lett.* **90**, 075501 (2003).
- ²J. A. TenCate and T. J. Shankland, *Geophys. Res. Lett.* **23**, 3019 (1996).
- ³J. A. TenCate, E. Smith, and R. A. Guyer, *Phys. Rev. Lett.* **85**, 1020 (2000).
- ⁴P. A. Johnson and A. Sutin, *J. Acoust. Soc. Am.* **117**, 124 (2005).
- ⁵M. Bentahar and R. El Guerjouma (unpublished).
- ⁶K. van den Abeele and J. De Vissche, *Cem. Concr. Res.* **30**, 1453 (2000). Here only fast dynamics have been considered.
- ⁷J. A. TenCate, D. Pasqualini, S. Habib, K. Heitmann, D. Higdon, and P. A. Johnson, *Phys. Rev. Lett.* **93**, 065501 (2004).
- ⁸T. J. Ulrich and T. W. Darling, *Geophys. Res. Lett.* **28**, 2293 (2001).
- ⁹P. P. Delsanto and M. Scalerandi, *Phys. Rev. B* **68**, 064107 (2003).
- ¹⁰K. Van den Abeele, S. Sutin, and P. A. Johnson, *Res. Nondestruct. Eval.* **12**, 17 (2000); A. Moussatov, V. Gusev, and B. Castagnede, *Phys. Rev. Lett.* **90**, 124301 (2003).
- ¹¹H. M. Jaeger, S. R. Nagel, and R. P. Behringer, *Phys. Today* **20**(4), 32 (1996).
- ¹²F. Windels and K. van den Abeele, *Ultrasonics* **42**, 1025 (2004).
- ¹³B. Zinszner, P. A. Johnson, and P. N. J. Rasolofosaon, *J. Geophys. Res.* **102**, 8105 (1997).
- ¹⁴O. O. Vakhnenko, V. O. Vakhnenko, T. J. Shankland, and J. A. TenCate, *Phys. Rev. E* **70**, 015602(R) (2004).
- ¹⁵V. Aleshin and K. van den Abeele, *J. Mech. Phys. Solids* **53**, 795 (2005).
- ¹⁶C. Pecorari, *J. Acoust. Soc. Am.* **116**, 1938 (2004).
- ¹⁷V. Zaitsev, V. Gusev, and B. Castagnede, *Phys. Rev. Lett.* **90**, 075501 (2003).
- ¹⁸K. van den Abeele, P. A. Johnson, R. A. Guyer, and K. R. McCall, *J. Acoust. Soc. Am.* **101**, 1885 (1997); K. van den Abeele, F. Schubert, V. Aleshin, F. Windels, and J. Carmeliet, *Ultrasonics* **42**, 1017 (2004).
- ¹⁹P. P. Delsanto, S. Hirsekorn, V. Agostini, R. Loparco, and A. Koka, *Ultrasonics* **40**, 605 (2002).
- ²⁰V. Gusev and V. Aleshin, *J. Acoust. Soc. Am.* **112**, 2666 (2002); V. Gusev and V. Yu. Zaitsev, *Phys. Lett. A* **314**, 117 (2003).
- ²¹B. Capogrosso-Sansone and R. A. Guyer, *Phys. Rev. B* **66**, 224101 (2002).
- ²²M. Scalerandi, P. P. Delsanto, V. Agostini, K. Van Den Abeele, and P. A. Johnson, *J. Acoust. Soc. Am.* **113**, 3049 (2003); M. Scalerandi, P. P. Delsanto, and P. A. Johnson, *J. Phys. D* **36**, 288 (2003).
- ²³A. Baltazar, S. I. Rokhlin, and C. Pecorari, *J. Mech. Phys. Solids* **50**, 1397 (2002); J.-Y. Kim, A. Baltazar, and S. I. Rokhlin, *ibid.* **52**, 1911 (2004).
- ²⁴V. Gusev, *J. Acoust. Soc. Am.* **117**, 1850 (2005).
- ²⁵D. J. Holcomb, *J. Geophys. Res. B* **86**, 6235 (1981).
- ²⁶R. A. Guyer, K. R. McCall, and G. N. Boitnott, *Phys. Rev. Lett.* **74**, 3491 (1995).
- ²⁷P. P. Delsanto, M. Nobili, and M. Scalerandi, *Mater. Sci. Forum* **480-481**, 573 (2004).
- ²⁸M. Nobili and M. Scalerandi, *Phys. Rev. B* **69**, 104105 (2004).
- ²⁹J. C. Lacouture, P. Johnson, and F. Cohen-Tenoudji, *J. Acoust. Soc. Am.* **113**, 1325 (2003).
- ³⁰H. C. Wu and K. Warnemuende, *Proc. SPIE* **3995**, 501 (2000).
- ³¹K. Warnemuende and H. C. Wu, *Cem. Concr. Res.* **34**, 563 (2004).
- ³²I. Y. Solodov, *J. Acoust. Soc. Am.* **101**, 3081 (1997).
- ³³M. D. Collins, J. Finngvitch, and W. L. Serghmann, *Wave Motion* **25**, 265 (1997); N. P. Chotiros, *J. Acoust. Soc. Am.* **97**, 114 (1995).
- ³⁴A. S. Gliozzi, M. Nobili, and M. Scalerandi, in *The Universality of Nonclassical Nonlinearity with Applications to NDE and Ultrasonics*, edited by P. P. Delsanto (Springer, New York, 2005), Chap. 16.
- ³⁵M. Scalerandi, M. Nobili, M. Griffa, A. Gliozzi, and F. Bosia, Ref. 34, Chap. 17.
- ³⁶A. C. Pipkin, *Lectures on Viscoelasticity Theory* (Springer-Verlag, New York, 1986).
- ³⁷S. M. Day and J. B. Minster, *Geophys. J. R. Astron. Soc.* **78**, 105 (1984).
- ³⁸J. O. A. Robertsson, J. O. Blanch, and W. W. Symes, *Geophysics* **59**, 1444 (1994).
- ³⁹M. Caputo and F. Mainardi, *Pure Appl. Geophys.* **91**, 134 (1971).
- ⁴⁰H. Schiessel, R. Metzler, A. Blumen, and T. F. Nonnenmacher, *J. Phys. A* **28**, 6567 (1995).
- ⁴¹J. M. Carcione, F. Cavallini, F. Mainardi, and A. Haniga, *Pure Appl. Geophys.* **159**, 1719 (2002).
- ⁴²J. M. Carcione, F. Poletto, and D. Gei, *J. Comput. Phys.* **196**, 282 (2004).